Features Classification of EMG Signal Envelope Under Colored Noise

Sandra Márquez-Figueroa * **Yuriy S.Shmaliy** *
Oscar Ibarra-Manzano *

* *Department of Electronics Engineering*
Universidad de Guanajuato
Salamanca, 36885, México
Email: {s.marquez}{shmaliy}{ibarrao}@ugto.mx

Abstract: An analysis of the electromyography (EMG) signal features is provided to realize whether a subject has made some motion or not. In this paper we determine such features and specify the motion characteristics required in the prothesis robotics. An accurate features analysis requires the EMG signal envelope, which is highly affected by diverse artifacts and unknown non Gaussian noise. It is shown that noise and artifacts can be efficiently suppressed if to use filtering algorithms developed for colored measurement noise (CMN). An efficient filtering algorithm is presented to remove the EMG envelope artifacts. It is also demonstrated that the EMG signal features can be extracted with more accuracy under the CMN. Extensive experimental investigations are provided using diverse EMG signal data.Feature analysis in biomedical signals often requires the calculation of the envelope. However, envelope acquisition methods extract undesirable artifacts; Therefore, many researchers develop extraction techniques. We will present filtration processes to remove EMG envelope artifacts, which estimates the linear envelope of the signal at the output. Finally, we will know if the EMG envelope gives the optimal features for an accurate prediction.

Keywords: EMG signals, envelope, filtering, features, classification.

1. INTRODUCTION

Electromyography (EMG) is a recording of potentials of the different muscle fibers, which records positive and negative deflections of the electrical activity or signals from a particular muscle, where we can visualize the performance of the data. EMG signals are represented in real-time for a better analysis. The EMG analysis can be combined with different technologies for a better result to identify the information that may interest us. To effectively do that, we also need to remove the noise which comes from the surrounding electricity, unwanted detail from waveforms have to be eliminated and reduced by using of good quality filter digital (1; 2; 3). The extracted information from EMG singal is used by bio-electronics, bio-mechanics, and biorobotics applications, where uses EMG features as such as frequency and amplitude to identify diverse motions (4; 5; 6).

For better qualitative analysis of the EMG recording , the EMG envelope is getting by using different methods, where the value negative else becomes positive (5; 11; 12; 13).Some research uses the envelope, which is reflected in the average movement activity, thus achieving an efficient noise reduction. However, it produces unacceptable bias errors and does not prevent spikes (14; 15). In (16), the envelope improves using the Savitsky-Golay smoother combined with a low-pass filter, the smoothing provides. However, it introduces time-delay-lags. In this investigation, we employ the NinaPro database, which contains the records of the upper limbs of 27 intact subjects while performing 52 finger, hand and wrist movements of interest (28). The data resolution over a 10 mV range. A part of the EMG signal record is given in Fig. 1. The EMG signal morphology is clearly recognized. All tests of synthetic data are provided using a special software.

2. EMG SIGNAL ENVELOPE AND PROBLEM FORMULATION

2.1 EMG Signal Envelope

The Hilbert Transformation is a mathematical algorithm to provide the EMG signal envelope. The Hilbert transformation $\hat{u}_n$ (imaginary part) of u_n (real part) can be used to draw the envelope $U_n = \sqrt{u_n^2 + \hat{u}_n^2}$, as shown in Fig.1, available from (24), where desired (smoothed) envelope is required due to the data are highly contaminated by noise (15). Several important observations can now be made by analyzing Fig. 1:

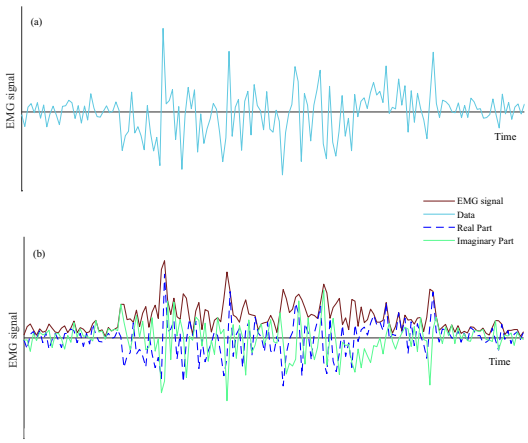

Fig. 1. Envelope shaping of an EMG signal having low MUAP density (24): (a) measured waveform and (b) envelope shaping, where the original data are depicted with a dashed line, the Hilbert transform (imaginary signal) with a solid line, and an envelope with a bold line.

The problem focuses on identifying the best processing algorithm achieving the highest estimation, in order to increase the accuracy of the features. Therefore, we make a comparison between traditional filters and modified filters assuming CMN using advanced statistical techniques. Thus, our report can be better geared towards the monitoring and evaluation of its trends.

3. EMG ENVELOPE MODEL AND FILTERING ALGORITHMS

This section shows a method of extracting the envelope of the signals with the different motions, for which the features are extracted to determine what kind of movement it belongs. We start with the NinaPro database, which contains kinematic and sEMG data from the upper limbs of 27 intact subjects while performing 52 finger, hand and wrist movements of interest. This database is publicly available for academic purposes at a dedicated website (28). At last, We developed the algorithms to produce estimates with minimal variations about the desired smooth envelope and insignificant time-delays.

3.1 State-Space Model of EMG Signal Envelope

For discreet case, U_n can be formulated in the state space with

$$x_n = Ax_{n-1} + Bw_n\,, \tag{1}$$
$$y_n = Hx_n + v_n\,, \tag{2}$$
$$v_n = \psi_n v_{n-1} + \xi_n\,, \tag{3}$$

For polynomial approximation, entries of the system matrix A are provided by the Taylor series (30; 31),

$$A = \begin{bmatrix} 1 & \tau & \frac{\tau^2}{2} & \dots & \frac{\tau^{K-1}}{(K-1)!} \\ 0 & 1 & \tau & \dots & \frac{\tau^{K-2}}{(K-2)!} \\ 0 & 0 & 1 & \dots & \frac{\tau^{K-3}}{(K-3)!} \\ \vdots & \vdots & \vdots & \ddots & \vdots \\ 0 & 0 & 0 & \dots & 1 \end{bmatrix} \in R^{K\times K}, \tag{4}$$

where n is the discrete-time index, K is the number of the envelope states, $x_n \in R^K$ is the state vector, y_n is the scalar observation of U_n, ψ_n is the scalar color factor, w_n is the envelope noise, v_n is the system noise, δ_n is a Kroneker symbol, which has unknown entries, the observation matrix is $H = [1\,0\dots0] \in R^{1\times K}$. Matrix $B_n \in R^{K\times P}$ projects the envelope noise $w_n \in R^P$ into x_n. ψ_n is supposed to be known at each n and such that noise v_n is stationary; by $\psi_n = 0$, noise v_n becomes white Gaussian, as required by optimal estimators. Due to w_n, is generally unknown, it is supposed to have zero mean with uncertain both the statistics and distribution. However, to run the KF, we will consider w_n as zero mean and white Gaussian, $w_n \sim \mathcal{N}(0, Q) \in R^P$, with the covariance $E\{w_n w_k^T\} = Q\delta_{n-k}$.Noise ξ_n is zero mean and white Gaussian, $\xi_n \sim \mathcal{N}(0, \sigma_n^2)$, with the variance $E\{\xi_n^2\} = R = \sigma_\xi^2$ and the property $E\{w_n\xi_k\} = 0$ for all n and k. We assume that the estimate $\hat{x}_n\hat{x}_{n|n}$ of x_n under the intensive nonwhite variations in U_n (Fig. 1) will range closer to the desired envelope under the supposedly CMN.

3.2 cKF and cH$_\infty$ Algorithms

To apply the KF to (1)–(3), one can follow (**?**), consider a new observation z_n as measurement differences, and write

$$\begin{aligned} z_n &= y_n - \psi y_{n-1}\,, \\ &= Hx_n + v_n - \psi Hx_{n-1} - \psi v_{n-1}\,. \end{aligned} \tag{5}$$

By taking x_{n-1} from eq1 and v_{n-1} from (3), a new observation can be written as

$$z_n = Dx_n + \bar{v}_n\,, \tag{6}$$

where $D = H - \Gamma$, $\Gamma = \psi HF^{-1}$, and

$$\bar{v}_n = \Gamma Bw_n + \xi_n \tag{7}$$

is white Gaussian scalar noise with the properties,

$$E\{\bar{v}_n^2\} = \Gamma\Phi + R = \Gamma\Phi + \sigma_\xi^2\,, \tag{8}$$
$$E\{\bar{v}_n w_n^T\} = \Gamma BQ\,, \tag{9}$$

where the weighted matrix Q is

$$\Phi = BQB^T\Gamma^T\,. \tag{10}$$

The modified state-space model (1) and (6) has now time-correlated and white w_n and $\bar{v}_n$ and the KF can be applied, if to derive the optimal bias correction gain

taking into account the correlation. For given y_n, $\hat{x}_0$, P_0, Q, R, ψ, and CMN, the cKF algorithm becomes

$$z_n = y_n - \psi y_{n-1}\,, \tag{11}$$
$$P_n^- = FP_{n-1}F^T + BQB^T\,, \tag{12}$$
$$S_n = DP_n^- D^T + R + H\Phi + \Phi^T D^T\,, \tag{13}$$
$$K_n = (P_n^- D^T + \Phi)S_n^{-1}\,, \tag{14}$$
$$\hat{x}_n^- = F\hat{x}_{n-1}\,, \tag{15}$$
$$\hat{x}_n = \hat{x}_n^- + K_n(z_n - D\hat{x}_n^-)\,, \tag{16}$$
$$P_n = (I - K_nD)P_n^- - K_n\Phi^T \tag{17}$$

and, by $\psi = 0$ and $\Phi = 0$, it becomes the standard KF.

The H_∞ filter has been derived based on the game theory in (29) as

$$\bar{P}_n = \bar{P}_n^-(I - \theta\bar{S}_n\bar{P}_n^- + H^T\bar{R}^{-1}H\bar{P}_n^-)^{-1}\,, \tag{18}$$
$$K_n^\infty = \bar{P}_nH^T\bar{R}^{-1}\,, \tag{19}$$
$$\hat{x}_n = F\hat{x}_{n-1} + K_n^\infty(y_n - HF\hat{x}_{n-1})\,, \tag{20}$$
$$P_{n+1}^- = F\bar{P}_nF^T + \bar{Q} \tag{21}$$

where chosen by the designer the symmetric positive definite matrices $\bar{P}_0$, $\bar{Q}$, and $\bar{R}$ have different meanings than in the KF and $\bar{P}_1^-$ can be computed as $\bar{P}_1^- = FP_0F^T + Q$ (29). Matrix $\bar{S}_n$ is constrained by a positive definite matrix $(\bar{P}_n^-)^{-1} - \theta S_n + H^T\bar{R}^{-1}H > 0$ in order to keep (18) positive definite. It is a user choice to assign $\bar{S}_n$, which is introduced in the cost function J to weight the estimation error. If a goal is to weight all error components equally, one must set $S_n = I$. Because the squared norm error-to-error ratio (cost J) is guaranteed in the H_∞ filter to be $J < 1/\theta$, a scalar bound $\theta > 0$ must be small enough. For Gaussian noise with no disturbances, $\theta = 0$ makes the H_∞ filter KF. For cH_∞, a new observation can be represented in discrete-time state-space as eq1.

3.3 cUFIR Filtering Algorithm

The UFIR filter (25) requires the zero mean assumption and an averaging horizon $[m, n]$ of N points, from $m = n - N + 1$ to n, to be optimal N_{opt} in the MSE sense. The advantage of this filter is that it does not require any information about the noise. Of importance is that w_n and $\bar{v}_n$ are both zero mean and their correlation does not produce bias. Therefore, this filter can be applied directly to (1) and (6), unlike the KF. The cUFIR algorithm operates as follows. Given N, y_n, and ψ, one must set $n = N-1, N, \ldots$, $m = n - N + 1$, and $s = n - N + K$ and compute the initial values $G_s = (C_{m,s}^T C_{m,s})^{-1}$ and $\bar{x}_s = G_sC_{m,s}^T Y_{m,s}$ in short batch forms via $Y_{m,s} = [\,y_m \;\ldots\; y_s\,]^T$ and

$$C_{m,s} = \begin{bmatrix} DA^{-(K-1)} \\ \vdots \\ DA^{-1} \\ D \end{bmatrix}. \tag{22}$$

Provided the initial values at s, iteratively updated values appear for $l = s+1, \ldots, n$ using the recursions

$$z_l = y_l - \psi y_{l-1}\,, \tag{23}$$
$$G_l = [D^TD + (AG_{l-1}A^T)^{-1}]^{-1}\,, \tag{24}$$
$$K_l = G_lD^T\,, \tag{25}$$
$$\bar{x}_l^- = A\bar{x}_{l-1}\,, \tag{26}$$
$$\bar{x}_l = \bar{x}_l^- + K_l(z_l - D\bar{x}_l^-)\,, \tag{27}$$

and the output estimate $\hat{x}_n = \bar{x}_n$ is taken when $l = n$. It also follows that, by $\psi = 0$, the cUFIR algorithm becomes the standard UFIR filter. The error covariance of the UFIR filter can be computed approximately by the KF error covariance if to replace the Kalman gain K_n with G_nD^T. That yields

$$\begin{aligned} P_n &= (I - G_nD^TD)P_n^-(I - G_nD^TD)^T \\ &\quad + G_nD^T(\Gamma\Phi + R)DG_n \\ &\quad - 2(I - G_nD^TD)\Phi DG_n \\ &= P_n^- - 2(P_n^-D^T + \Phi)DG_n + G_nD^TS_nDG_n \\ &= P_n^- - (2P_n^-D^T + 2\Phi + G_nD^TS_n)DG_n\,, \end{aligned} \tag{28}$$

where P_n^- is given by (12) and S_n by (13). Note that the cUFIR algorithm does not require P_n, although the recursion (28) can be included to for any purposes.

4. APPLICATIONS

We will apply the cKF, cH_∞, and cUFIR algorithms, which are compared to the KF, H_∞ filter, and UFIR filter. First, we will consider EMG signals to determine if they have any indications, signs, symptoms, diagnosis or treatment of any disease, disorder, or abnormality, for which we require the Hilbert transform to shape the envelope. Next, we will identify their features. For all EMG data, we specify model (1)–(3) with two states, $K = 2$, and matrices

$$A = \begin{bmatrix} 1 & \tau \\ 0 & 1 \end{bmatrix}, B = \begin{bmatrix} \dfrac{\tau^2}{2} \\ \tau \end{bmatrix}, H = [\,1\;0\,]\,. \tag{29}$$

We suppose that the envelope noise w_n acts in the third state and projects to state x_n by matrix B. The filters will be applied to EMG signal data available from (27; 28).

4.1 EMG Signals Processing to Determine Motions

First Application :

We begin with a surface EMG signal collected from the basic movements of the fingers made by a 28-year-old

man, database available at (28). Fig.2a shows the Hilbert transform getting from healthy raw EMG, as well as in Fig. 2b and Fig.2c show the envelopes shaped by each standard filter. In Fig. 2b, we apply developed algorithms on the envelope using a $N_{\text{opt}} = 140$ for the UFIR filter and supuse a standard deviation of $\sigma_\xi = 50\,\mu\text{V}$ and set $\sigma_w = 0.1\,\text{V/s}^2$ for the KF estimate. For the H_∞ filter, we consider the case of $S_n = I.$ and $\theta = 1.0e^{-6}$. It is imperative to keep in mind mention that $0 < \theta < 1$ must be small enough to provide better robustness than by the KF (29).

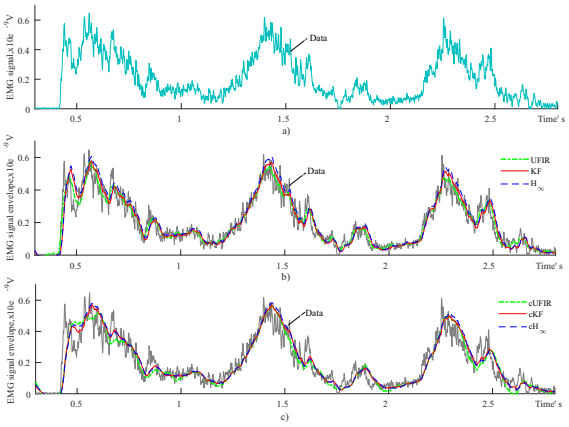

Fig. 2. A part of the EMG signal (0.3...2.8)s available from (27): a) envelope (data) obtained through the Hilbert transform (solid), b) its UFIR (dash-dotted), KF (bold), and H_∞ (dashed) estimates, and c) cUFIR (dash-dotted), cKF (bold), and cH_∞ (dashed line) estimates.

In Fig. 2c can be observed as the excursions are suppressed by the cKF, the cH$_\infty$, and cUFIR using $\psi = 0.65$, $\theta = 1.0e^{-6}$, and $N_{\text{opt}} = 140$. We have found all values experimentally.

Second Application :

We now consider an EMG signal with grasping and functional movements, which were taken from a 31-year-old man(28). The selected part of a signal shown in Fig. 3b was processed similarly to the previous case with the same tuning parameters. As can be seen, the KF, H_∞ filter, and UFIR filter still produce consistent estimates with no essential time-delays. It can also be concluded that the cKF, cH_∞, and cUFIR filter better suppress the excursion, this may be seen in Fig. 3c with $\psi_{\text{opt}} = 0.65$.

Third Application :

The third motion is shown by Fig.4, which show the made estimations by each developed algorithm in this paper. At last, we can only conclude that again Gauss-Markov interpretation of variations in the EMG signal allows getting a more smoothed envelope. Other important conclusions are as follow:

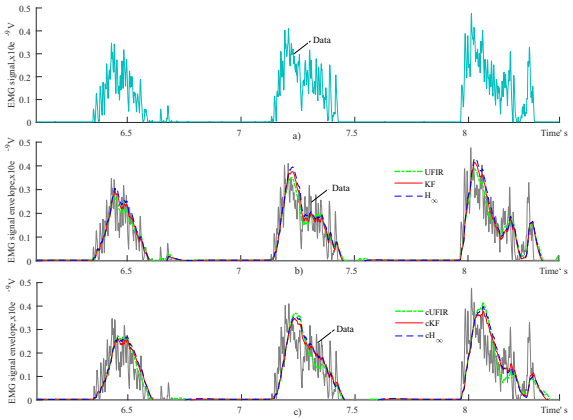

Fig. 3. A part of the EMG signal (6.2...8.6)s available from (28): a) envelope (data) obtained through the Hilbert transform (solid), b) UFIR (dash-dotted), KF (bold), and H_∞ (dashed) estimates, and c) cUFIR (dash-dotted), cKF (bold), and cH_∞ (dashed line) estimates.

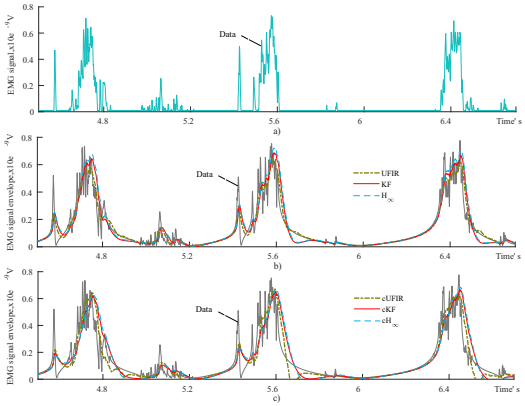

Fig. 4. A part of the EMG signal (4.5...6.7)s available from (27): a) envelope (data) obtained through the Hilbert transform (solid), b) its UFIR (dash-dotted), KF (bold), and H_∞ (dashed) estimates, and c) cUFIR (dash-dotted), cKF (bold), and cH_∞ (dashed line) estimates.

4.2 Classification of Features

One way to evaluate the EMG signal is to segment the transient waveform and determine its features statistically, which can be done using several available methods. In this paper, we extract features of amplitude, time, and frequency by applying the Hilbert transform (34). The most common time domain features of EMG signals are listed in Table I.

The classification model using in this paper is the Quadratic SVM with a multiclass method of one-vs-one. We can only conclude that the features classification of

Table 1. Feactures of the EMG signal

Time Domain Feacture	
Integrated EMG	$IEMG = \sum_{n=1}^{N} \|x_n\|$
Mean Absolute Value	$MAV = \frac{1}{N} \sum_{n=1}^{N} \|x_n\|$
Root MEan Squere	$RMS = \sqrt{\frac{1}{N} \sum_{n=1}^{N} x_n^2}$
Waveform Length	$WL = \sum_{n=1}^{N-1} \|x_{n+1} - x_n\|$
Standard Deviation	$STD = \sqrt{\frac{1}{N} \sum_{n=1}^{N-1} (x_n - \overline{x})^2}$

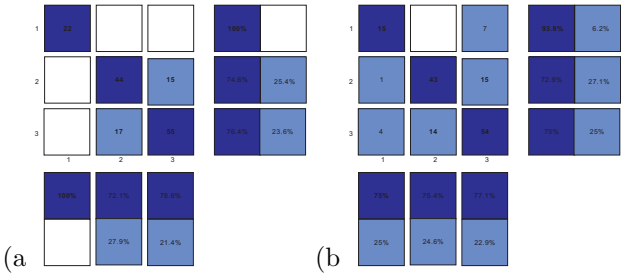

(a (b

Fig. 5. cUFIR Filter Confusion Matrix and KF Filter Confusion Matrix

the modified algorithms is better than that of the standard filters, which is visible in the confounding matrices shown in this section. First, the confusion matrix of the cUFIR filter is showed in Fig.5a and then the confusion matrix of the KF algorithm is showed in Fig.5b. Given an accuracy of 79.1% and 73.2%, respectively. The above test was repeated for each estimation reaping the same success. It is important to mention that features are not free from outliers.

In Fig.5a and Fig.5b, the first three diagonal cells show the number of correct classifications, where 153 data have been used by motions classification technical. From Fig.5a, the following can be noted, 22 cases are correctly classifed as motion 1. This corresponds to 100% . Similarly, 44 cases are correctly classified as motion 2 and 55 cases as motion 3. This corresponds to 74.6% and 76.4% of all, respectively. 15 of the data are incorrectly classified as motion 3 and this corresponds to 25.4% of all in motion 2. Similarly, 17 of motion 3 are incorrectly classified as motion 2 and this corresponds to 23.6% of all data in motion 3. Overall, 79.1% of the data are correct and 20.9% are wrong classifications.

On Fig.5b, out of 153 data, 73.2% are correct and 26.8% are wrong. Out of 22 data of motion 1, 93.8% are correct and 6.2% are wrong. Out of 59 motion 2 cases, 72.9% are correctly predicted as motion 2 and 27.1% are predicted wrong. Out of motion 3, 95% are correct and 25% are classified wrong.

5. CONCLUSIONS

The envelope is not artifact-free, in respect of which tend to be high variations that can be seen by the naked eye. Once the filtered envelope has been determined and calculated by using the different algorithms, one can conclude that the filters that are based on CMN mathematical approaches perform better under the WGN. The modified algorithms cKF, cH$_\infty$, and cUFIR have demonstrated better performance into feature classification than the KF, H$_\infty$, and UFIR filters. It is clear that the outliers must be removed to get the best performance. Thus, these filters are more suitable for the desired envelop extraction, provided that the coloredness factor is chosen properly. The modified algorithms can further be improved to remove the outliers that we consider as a future work. Feature extraction and model processing are carried out by The Hilbert Transformation, but from the literature or other sources other methods of envelope getting are employed, it can be understood that the techniques reach similar results. The color factor ψ must be optimized to provide the best envelope shaping and ψ should not exceed 1.0 to satisfy the requirements of the measurement noise stationarity.

REFERENCES

[1] D. I. Rubin, J. R. Daube, Rapid MUAP quantization, in: AANEM Workshop, pp. 1–7, 2008.

[2] M. Reaz, M. Hussain, and F. Mohd-Yasin, "Techniques of emg signalanalysis: Detection, processing, classification, and applications," Biological Procedures Online, vol. 8, pp. 11–35, 2006.

[3] A. Merlo, D. Farina, and R. Merletti, "A fast and reliable technique formuscle activity detection from surface emg signals," IEEE Trans. Biomed. Eng, vol. 50, no. 3, pp. 316–323, 2003.

[4] G. Tallison, P. Godfrey, G. Robinson, "EMG signal amplitude assessment during abdominal bracing and hollowing," J. Elec- tromyography Kinesiology, vol. 8, no. 1, pp. 51–57, 1996.

[5] T. D'Alessio and S. Conforto, "Extraction of the envelope from surface EMG signals," IEEE Eng. Med. Biol. Mag., vol. 20, no. 6, pp. 55–61, 2001.

[6] L. Zhang, R. Shiavi, M. A. Hunt and J. Chen, "Clustering analysis and pattern discrimination of EMG linear envelopes," IEEE Trans. Biomed. Eng, vol. 38, no. 8, pp. 777-784, Aug. 1991.

[7] S. Thongpanja, A. Phinyomark, F. Quaine, Y. Laurillau, C. Limsakul, and P. Phukpattaranont, "Probability density functions of stationary surface EMG signals in noisy environments," IEEE Trans. Inf. Theory, vol. 63, no. 6, pp. 1547–1557, 2016.

[8] G. Jang, J. Kim, S. Lee, and Y. Choi, "EMG-based continuous control scheme with simple classifier for electric-powered wheelchair," IEEE Trans. Instrum. Elec., vol. 65, no. 7, pp. 3695–3705, 2016

[9] L. Ramírez, M. Ruano, C. Younes, "Análisis de bioseñales: Enfoque téecnico en el an álisis clínico de señales fonocardiográaficas, 1st Edition," Univ. Nacional de Colombia, vol. 1, pp. 1–1, 2016.

[10] V. de A. Rocha, J. C. do Carmo and F. Assis de O. Nascimento, "Weighted-Cumulated S-EMG Muscle Fatigue Estimator," IEEE J. Biomedical and Health Informatics, vol. 22, no. 6, pp. 1854-1862, Nov. 2018.

[11] H. Xie, Z. Wang, "Mean frequency derived via Hilbert-Huang transform with application to fatigue EMG signal analysis," Computer Methods and Programs in Biomedicine, vol. 82, no.2, pp. 312–320, 2006.

[12] P. Kutilek, J. Hýbl, J. Mareš, V. Socha, P.Smrcka, Pavel, "A myoelectric prosthetic arm controlled by a sensor-actuator loop," Acta Polytechnica, vol. 54, pp.197-204, 2014.

[13] L. Chen and H. Yaru, "Feature extraction and classification of ehgbetween pregnancy and labour group using hilbert-huang transform andextreme learning machine," Computational and Mathematical Methodsin Medicine, vol. 2017, pp. 1–9, 02 2017.

[14] R. Kleissen and G. Zilvold, "Estimation uncertainty in ensemble averagesurface emg profiles during gait," J. Electromyography Kinesiology, vol. 4, pp. 83–94, 1994

[15] I. Stirn, T. Jarm, Tomaz, V. Peter Kapus, V. Strojnik, "Evaluation of mean power spectral frequency of EMG signal during 100 metre crawl," Europ. J. Sport Science, vol.13, pp. 1-10, 2011.

[16] Y. Chien Hung, H. Wen Vincent Young, C.Yen Wang, Y. HungWang, P. Lei Lee, J. Horng Kang, and M. Tzung Lo, "Quantifying spasticity with limited swinging cycles using pendulum test based onphase amplitude coupling," IEEE Trans. Nucl. Sci, vol. 24, pp. 1–1, 2016.

[17] R. M. Studer, R. J. P. Figueiredo, G. S. Moschytz, "An algorithm for sequential signal estimation and system identification for EMG signals", IEEE Trans. Biomed. Eng, vol. 31, no.3, pp.285-295, 1984.

[18] Y. Zhan, S. Guo, K. M. Kendrick, J. Feng, "Filtering noise for synchronised activity in multi-trial electrophysiology data using Wiener and Kalman filters," BioSystems, vol.96, no.1, pp.1–13, 2009.

[19] N. M. Ĺopez, F. di Sciascio, C. M. Soria, M. E. Valentinuzzi, "Robust EMG sensing system based on data fusion for myoelectric control of a robotic arm," BioMedical Eng OnLine, vol.8, no.5, pp. 1-13, 2009.

[20] C. S. L. Tsui, J. Q. Gan, S. J. Roberts, "A self-paced braincomputer interface for controlling a robot simulator: an online event labelling paradigm and an extended Kalman filter based algorithm for online training," Med Biol Eng Comput, vol. 47, no.3, pp.257-265, 2009.

[21] L. L. Menegaldo, "Real-time muscle state estimation from EMG signals during isometric contractions using Kalman filters," Biol Cybern, vol. 111, no. 5-7, pp. 335–346, 2017.

[22] T. Triwiyantoa, O. Wahyunggoroa, H. A. Nugrohoa, H. Herianto, "Muscle fatigue compensation of the electromyography signal for elbow joint angle estimation using adaptive feature," Computers Electr. Eng., vol. 71, pp. 284–293, 2018.

[23] K. Uribe-Murcia, Y. S. Shmaliy, C. K. Ahn and S. Zhao, "Unbiased FIR Filtering for Time-Stamped Discretely Delayed and Missing Data," in IEEE Transactions on Automatic Control.2019.

[24] O. Aviles, J. Rodriguez, M. Herrera, G. Martinez, UCI Machine Learning Repository. Bogota: Iniversidad Militar Nueva Granada, Tecno Parque SENA nodo Manizales, 2012.

[25] Y. Shmaliy, "An iterative kalman-like algorithm ignoring noise and initialconditions," IEEE Trans. Signal Process., vol. 59, pp. 2465–2473, 2011.

[26] Watson JC, Dyck PJ. Peripheral Neuropathy: A Practical Approach to Diagnosis and Symptom Management. Mayo Clin Proc 2015;90:940-51.

[27] Goldberger AL, Amaral LAN, Glass L, Hausdorff JM, Ivanov PCh, Mark RG, Mietus JE, Moody GB, Peng C-K, Stanley HE. PhysioBank, PhysioToolkit, and PhysioNet: Components of a New Research Resource for Complex Physiologic Signals (2003). Circulation. 101(23):e215-e220.

[28] Atzori M., Gijsberts A., Heynen S., Mittaz Hager A.-G., Deriaz O., Van der Smagt P., Castellini C., Caputo B., and Müller H. 2012 IEEE International Conference on Biomedical Robotics and Biomechatronics (BioRob 2012).

[29] Y. S. Shmaliy, F. Lehmann, S. Zhao, and C. K. Ahn, "Comparing robustness of the kalman, H_∞, and UFIR filters," IEEE Trans. Signal Process, vol. 66, no. 13, pp. 3447–3458, 2018.

[30] Y. S. Shmaliy, "Unbiased FIR filtering of discrete time polynomial state space models," *IEEE Trans. on Signal Process.*, vol. 57, no. 4, pp. 1241-1249, 2009.

[31] Y. Shmaliy, A. Marienko, and A. Savchuk, "Gps-based optimal kalmanestimation of time error, frequency offset, and aging," 31st Precise Time and Time Interval (PTTI) Systems and Application Mtg, pp. 431–440, 1999.

[32] S. Marquez-Figueroa, Y. S. Shmaliy, and O. Ibarra-Manzano, "Optimal extraction of EMG signal envelope and artifacts removal assuming colored measurement noise," *Biomed. Signal Process. Control*, vol. 57 (to be published).

[33] M. Atzori, A. Gijsberts, C. Castellini, B. Caputo, H. A. Mittaz, S. Elsig, G. Giatsidis, F. Bassetto, H. Müller, Electromyography data for non-invasive naturally controlled robotic hand protheses. Scientific Data 1:140053 (2014). URL https://doi.org/10.1038/sdata.2014.53

[34] Lyu, M., Chen, W.-H., Ding, X., Wang, J., Pei, Z., Zhang, B. (2019). Development of an EMG-Controlled Knee Exoskeleton to Assist Home Rehabilitation in a Game Context. Frontiers in Neurorobotics, 13.

